# Anisotropy of the nuclear magnetic relaxation times induced in solid 3He by modulation of the dipolar interactions

G. Deville

Classification
*Physics Abstracts*
7.750

# ANISOTROPY OF THE NUCLEAR MAGNETIC RELAXATION TIMES INDUCED IN SOLID $^3$He BY MODULATION OF THE DIPOLAR INTERACTIONS (*)

G. DEVILLE

Service de Physique du Solide et de Résonance Magnétique,
Centre d'Etudes Nucléaires de Saclay, B.P. 2, 91190 Gif-sur-Yvette, France

(*Reçu le 5 novembre 1975, révisé le 9 février 1976, accepté le 16 février 1976*)

**Résumé.** — On présente des mesures de temps de relaxation magnétique nucléaire anisotropes dans des échantillons d'hélium trois solide fabriqués à pression constante, qui ont été réalisées aux fréquences de Larmor comprises entre 1,5 MHz et 5 MHz et lorsque le mécanisme dominant dans la relaxation est la modulation de l'interaction dipolaire par l'échange ou le mouvement des lacunes. Le calcul au second ordre fait par Harris dans le cas où la relaxation est dominée par l'échange est étendu au régime pour lequel c'est le mouvement des lacunes qui l'emporte. On complète ensuite la théorie en considérant l'effet de l'anisotropie du quatrième moment sur les densités spectrales. Ce calcul fait ressortir une contribution anisotrope à $T_1$ qui est fonction de la fréquence de Larmor. Ce fait est en accord qualitatif avec nos mesures contrairement aux résultats plus simples obtenus par Harris.

**Abstract.** — Anisotropic nuclear relaxation times have been measured in solid $^3$He samples grown at constant pressure, in the Larmor frequency range 1.5 MHz-5 MHz and where the main relaxation mechanism is the modulation of the dipolar interaction by exchange or by motion of the vacancies. The second order calculation made by Harris for the exchange induced relaxation regime is extended to the regime where vacancy motion dominates. The theory is further refined by considering the fourth moment anisotropy effect on the spectral densities. This latter calculation yields a frequency dependent anisotropic contribution to $T_1$ which agrees qualitatively with the data, unlike the simpler results by Harris.

1. **Introduction.** — Most of the NMR studies of solid helium three have been performed with samples grown by the blocked capillary method [1, 2, 3]. This simple method produces solids of well defined molar volume but, as the crystallization is realized by nucleation in bulk liquid, it is excepted to generate a few single crystals which are probably randomly orientated [4]. One is therefore justified in considering these samples as powders and, in particular, performing the angular averages over all possible orientations when calculating relaxation times. Actually, most of the NMR experimental results are in agreement with such a hypothesis [5]. It is also known that near its melting temperature, solid helium three contains a large number of thermally excitated and very mobile vacancies [6] which facilitate the atomic motions and the solid exhibits an important tendency to anneal [7]. An anisotropic transverse relaxation time was reported for the first time to our knowledge by Giffard *et al.* [8] who studied a sample grown by the blocked capillary method : it was a body centered cubic $^3$He crystal whose molar volume was $V_m = 20$ cm$^3$ and it exhibited an anisotropy

$$K_2 = \frac{\Delta(1/T_2)}{(1/T_2)} \sim 0.15$$

at the Larmor frequency $\omega/2\pi = 1.9$ MHz and at the temperature $T = 0.89$ K. In this experiment the anisotropic feature was the only sign of the monocrystalline state of the sample. However, the $K_2$ value just as the $T_2$ dependence on the magnetic field orientation were consistent with the expected anisotropic relaxation times [9] for a single crystal deduced from the anisotropy of the second moment of the resonance line [10].

The properties of solid helium have been extensively studied in other fields : measurements of the thermal conductivity [11], sound propagation [12, 13, 14] and ionic mobilities [15], which require high quality monocrystalline samples. New constant pressure

(*) Part of a thesis to be presented by the author at the Université Paris Sud-Orsay for the degree of Docteur ès Sciences. Thesis registered with the C.N.R.S. as No. Ao 10042.

growing techniques have been used in which the temperature of the filling capillary is maintained slightly above the melting temperature of the solid [11] in order to avoid the blocking of the capillary. The crystal is thereby grown under a temperature gradient with a well defined solid-liquid interface. In many experiments the growing and the crystal quality are controlled separately by either direct observation [13] or measurement of the optical birefringence [12] while the crystal orientation is determined either by X rays [13] or optical birefringence techniques [12]. The latter techniques for determining the orientation of the crystal are determined by the nature of the measurements undertaken but, by no means, can they be used for testing the crystal quality. For instance, a sample could exhibit an excellent Laue photograph, it could be perfectly transparent and yet still be inadequate for a sound propagation experiment. This result shows that the test of crystal quality depends on the kind of measurements envisaged. The monocrystalline assumption is verified only through the interpretation of the experimental results.

The aim of this paper is to present NMR relaxation measurements carried out for $^3$He crystals grown at constant pressure. Most of our numerous data show large $T_1$ and $T_2$ anisotropies when rotating the magnetic field with respect to crystal axis. Unlike the work in references [12] and [13], we did not use an additional method to test the crystal quality and for this reason the NMR results can not be compared with independent data. Nevertheless, the analysis of the NMR relaxation features is consistent with a single crystal assumption and we believe that most of our samples were monocrystalline.

After a short description of the apparatus and the crystal growing technique we present the experimental results obtained in the Larmor frequency range 1.5 MHz-5 MHz and in the two crystalline phases : body centered cubic (bcc) and hexagonal closed packed (hcp). The comparison of these results with Harris's theory [9] leads to a disagreement which is shown to be partially lifted when the anisotropy of the fourth moment is included in the dipole energy correlation function.

2. **Experimental techniques.** — The apparatus has been already described briefly in a previous paper [6]. As we did not use a $^3$He refrigerator, the lowest temperature obtained in the present apparatus with pumped $^4$He was about 1 180 mK. We used a coherent pulsed NMR spectrometer operating between 1.5 MHz and 5 MHz. The pulse sequences we used were either a 90°-90° sequence in $T_1$ measurements [16] or a 90°-180° or a multiple pulses sequence 90°-180°-180°... 180° [17] in $T_2$ measurements. The data were obtained with an accuracy of the order of 1 to 2 % for $T_1$ and 3 % for $T_2$. The $^4$He concentration was less than 250 ppm but no attempt has been made to purify commercial $^3$He (Monsanto high purity grade $^3$He).

The experimental pressure cell was built using Kel-F. The sample chamber was cylindrical, having its axis aligned vertically, and was 6 mm in diameter and had a height of 10 mm, i.e. a 280 mm$^3$ volume. The pressure cell was thermally linked to the $^4$He bath by a copper plug which terminated in a finger at the bottom of the $^3$He sample. This copper finger produced a cold point where the crystallization was initiated. The $^3$He capillary entered the top of the cell and was thermally isolated by a 10 mm diameter tube which could be either pumped or filled with exchange gas. The last 10 cm of the capillary could also be heated by means of a 100 Ω resistor. Both the temperature and the temperature gradient were measured with the help of two thermometric carbon resistors : the first one, $R_1$, was inside the copper plug close to the bottom of the cell and the second one, $R_2$, was close to the end of the capillary, at the top of the cell. A feed-back system using $R_2$ as the sensor was used to monitor the capillary heating current when necessary.

GROWING OF CRYSTALS. — The most important process is to monitor the temperature gradient $\nabla T \propto (T(R_1) - T(R_2))$. The time evolutions of $T(R_1)$, $T(R_2)$ and $\nabla T$ during a crystal growth are shown in figure 1. The approximative time scale shows that

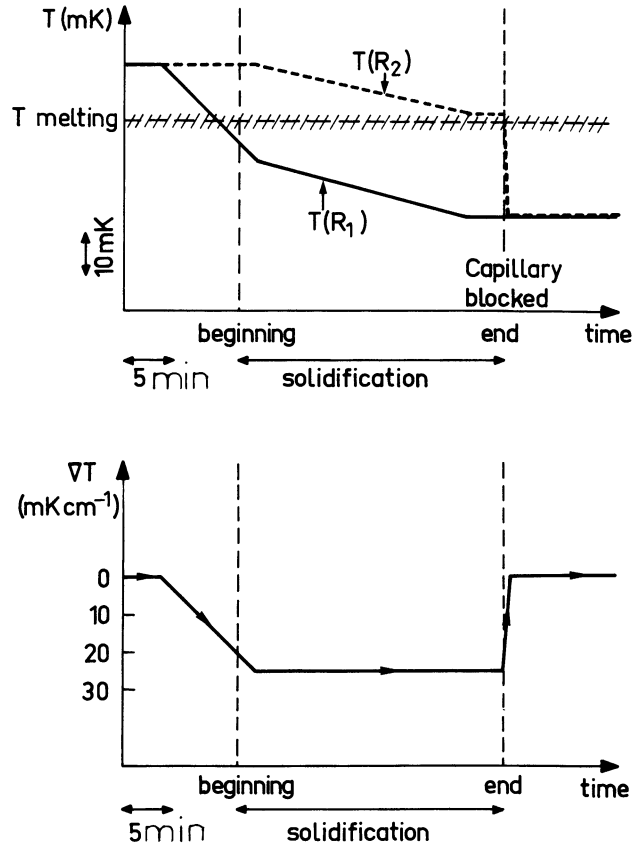


FIG. 1. — Variations of the temperature and of the gradient-temperature of the cell during a crystal growth. The values given are indicative as they can vary slightly from run to run. $T_m$ is the melting temperature of the solid at the chosen pressure. $T(R_2)$ is the upper cell temperature (capillary temperature) and $T(R_1)$ is the temperature of the bottom of the cell connected with the He$^4$ bath.

approximately 30 min is needed to grow a crystal from liquid helium three. $R_2$ is stabilized at about 20 mK above the melting temperature $T_m$ while the bottom of the cell is slowly cooled by pumping the $^4$He bath until the NMR signal appropriate for the solid appears. The signal for the solid is easily distinguished from that of the liquid since near $T_m$, and in our frequency range, the longitudinal relaxation time of liquid $^3$He is of the order of 100 s while it is only about 500 ms in bcc solid and 50 ms in hcp solid. Thus, saturation of liquid signal with recurrent 90° pulses renders only the signal of the solid visible. The increase of this solid signal observed on a memory oscillograph gives a direct picture of the crystal growth. When the solid signal appears, $T(R_1)$ is decreased more slowly while $T(R_2)$ is lowered until it almost reaches $T_m$. After checking on the oscillograph in order to ensure that the entire sample is in the solid phase, exchange gas is introduced in the capillary isolation tube; this lowers $T(R_2)$ suddenly below $T_m$ and the capillary is blocked and the growth of the crystal is completed. One can either anneal the crystal for a short or a long time or begin the measurements. Except for the electronic control of the capillary heating, all the processes described above are manual; the values of $T(R)$ or $\nabla T$ can therefore fluctuate slightly from run to run but this feature has no consequence on the crystal quality.

3. **Relaxation theory in $^3$He single crystals.** — In the temperature range of our experiments

$$4.2\ \mathrm{K} > T > 1.18\ \mathrm{K}\,,$$

the mechanism dominating the solid $^3$He relaxation is the modulation of the spin dipolar interaction by motion [4] : atomic motion due to vacancies or spin motion due to exchange interaction. The use of the energy-baths model [2] has proved to be very successful in accounting for the experimental results for the spin lattice relaxation time $T_1$. This model has been widely refined since and an *up to date* description can be found in reference [3]. We adopt their terminology for the motional relaxation regimes : the Z-VP regime refers to the direct relaxation of Zeeman energy by atomic motion when vacancies are numerous while the Z-EP regime observed at lower temperatures corresponds to the Zeeman-exchange cross relaxation. A comprehensive study of these two regimes is reported in references [18] and [19].

All the theories mentioned above apply to polycrystalline samples whose correlations functions are rather simple. To our knowledge, very few papers deal with spin relaxation induced by motion in single crystals. The random walk model [20] proposed by Torrey a long time ago as a description of the Z-VP regime in polycrystals has been extended by Wolf [21, 22] to correlated diffusion mechanisms in single crystals. We are aware of only one publication [9], already mentioned in the introduction, dealing with Z-EP regime in helium three single crystals. It gives a simple account of the anisotropic features, although it does not agree very well with our experimental results. As its predictions will help us in analysing the data, this theory is first reviewed and then we show that it can be easily extended to the Z-VP regime.

The dipolar hamiltonian [23]

$$\mathcal{H}_d = \sum_{i<j} \frac{\hbar\gamma^2}{r_{ij}^3}\left\{\mathbf{I}_i.\mathbf{I}_j - \frac{3}{r_{ij}^2}(\mathbf{I}_i.\mathbf{r}_{ij})\,(\mathbf{I}_j.\mathbf{r}_{ij})\right\}$$

can be written as a scalar product of spins and lattice tensor operators [18] :

$$\left.\begin{aligned}\mathcal{H}_d &= \sum_{m=-2}^{2} G_m \\ G_m &= \sum_{i<j}\sqrt{\frac{4\pi}{5}}\,\hbar\gamma^2\,\frac{Y_2^{-m}(\omega_{ij})}{r_{ij}^3}\,T_{ij}^m(-1)^m\,.\end{aligned}\right\} \quad (1)$$

$T_{ij}$ are spin operators :

$$\left.\begin{aligned}T_{ij}^0 &= \mathbf{I}_i.\mathbf{I}_j - 3\,I_i^z\,I_j^z \\ T_{ij}^1 &= \sqrt{\frac{3}{2}}\,(I_i^z\,I_j^+ + I_j^z\,I_i^+) = -\,(T_{ij}^{-1})^\dagger \\ T_{ij}^2 &= -\sqrt{\frac{3}{2}}\,(I_i^+\,I_j^+) = (T_{ij}^{-2})^\dagger\,.\end{aligned}\right\} \quad (2)$$

As a result of the large zero point motion, the distance $r_{ij}$ appearing in lattice operators is not the distance $R_{ij}$ between crystalline sites $i$ and $j$ but the thermal average of lattice operators can be written as :

$$\left\langle \frac{Y_2^m(\omega_{ij})}{r_{ij}^3}\right\rangle_R = \frac{Y_2^m(\Omega_{ij})}{R_{ij}^3}\,\xi(R_{ij})$$

where $\omega_{ij}$ defines the orientation of vector $\mathbf{r}_{ij}$, $\Omega_{ij}$ defines the orientation of vector $\mathbf{R}_{ij}$ and $\xi(R_{ij})$ is a renormalization function for the dipolar hamiltonian. The reader will find in reference [18] a discussion of the renormalization function. Let us postpone the consideration of the effect of this function and take $\xi(R_{ij}) = 1$. The calculation is then widely simplified and yields :

$$\frac{1}{T_1} = J_1(\omega) + 4\,J_2(2\,\omega) \quad (3)$$

$$\frac{1}{T_2} = \frac{3}{2}J_0(0) + \frac{5}{2}J_1(\omega) + J_2(2\,\omega) \quad (4)$$

with

$$J_m(\omega) = \int_{-\infty}^{\infty} g_m(t)\,\mathrm{e}^{-i\omega t}\,\mathrm{d}t$$

$$g_m(t) = \frac{4\,\pi\hbar^2\,\gamma^4}{5\,N}\sum_{i<j}\sum_{k<l} Y_2^{m*}(\Omega_{ij})\,Y_2^m(\Omega_{kl})\times \times\frac{1}{R_{ij}^3}\,\frac{1}{R_{kl}^3}\,\Gamma_{ijkl}(t)\,. \quad (5)$$

Up to this point, there has been no need to specify which of the Z-VP regime or of the Z-EP regime was being considered as the information about spin motion is contained in the correlation function $\Gamma_{ijkl}(t)$ to be defined later. As a first step we present Harris's calculation in which it is assumed that the angular dependence of $g_m(t)$ is wholly included in $g_m(0)$. We will show later that this simple theory can easily be extended to the Z-VP regime. Then, we drop Harris's assumption in order to take account of the anisotropy of the correlation function $\Gamma_{ijkl}(t)$. This leads to a frequency dependent $T_1$ anisotropy which is in good agreement with our data, contrary to the results predicted by Harris's simple theory. We shall make more comments on this point when describing the experimental data.

3.1 SECOND ORDER CALCULATION. — 3.1.1 Z-EP *regime* [9]. — The motion is expressed in terms of the exchange hamiltonian :

$$\mathcal{H}_e = -2 \sum_{i<j} J_{ij}\, \mathbf{I}_i . \mathbf{I}_j$$

$$\Gamma_{ijkl}(t) = \left(\frac{N}{\mathrm{Tr}\, I_z^2}\right) \mathrm{Tr}\, \{ T_{ij}^m\, e^{i\mathcal{H}_e t} (T_{kl}^m)^\dagger\, e^{-i\mathcal{H}_e t} \} . \quad (6)$$

This last expression is $m$ independent owing to the rotational invariance of $\mathcal{H}_e$. There are two types of terms : *like* terms such as $\Gamma_{ijij}(t)$ or *unlike* terms as $\Gamma_{ij\neq kl}(t)$ with different shapes as shown in figure 2. For like terms, the correlation is maximum at time zero and then decreases with a characteristic time of the order of $1/J$ while during the same time the unlike terms reach a maximum value under the effect of the exchange interactions. A straightforward calculation yields

$$\Gamma_{ijij}(0) = \frac{3}{2} \quad \text{while} \quad \Gamma_{ij\neq kl}(0) = 0 .$$

The Taylor expansion of the function $g_0(t)$ can easily be written in terms of moments of the absorption

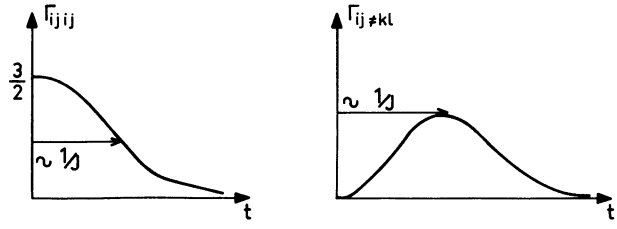


FIG. 2. — Approximative shapes of the two kinds of terms of the spin correlation function $\Gamma_{ijkl}(t)$ when the exchange interaction mechanism is dominant. For like terms, the correlation is maximum at time zero and then decreases with a characteristic time of the order of $1/J$ while during the same time the unlike terms reach a maximum value under the effect of the exchange interaction. The like terms $\Gamma_{ijik}$ contribute to the second moment $M_2$ and the fourth moment $M_4$ whereas the unlike terms only contribute to the fourth moment as $\Gamma_{ij\neq kl}(0) = 0$ .

resonant line whose Fourier transform is the free precession decay signal $G(t)$ [23]

$$G(t) = 1 - \frac{1}{2} M_2\, t^2 + \frac{1}{4!} M_4\, t^4 + \cdots .$$

Indeed, from :

$$g_0(t) \simeq -\frac{1}{3} \frac{d^2}{dt^2} G(t) = \frac{1}{3} \left[ M_2 - \frac{1}{2} M_4\, t^2 + \cdots \right]$$

one obtains the expressions for the second and the fourth moments $M_2$ and $M_4$ :

$$M_2 = 3\, g_0(0) \quad (7)$$

$$M_4 = -3\, \ddot{g}_0(0) \quad (8)$$

if we keep only the $J^2$ terms in the $M_4$ expression.

Observing that $\Gamma_{ij\neq kl}(0) = 0$, only products of the form $Y_2^{m*}(\Omega_{ij})\, Y_2^m(\Omega_{ij})$ appear in $g_m(0)$ which can be written as [24] :

$$Y_2^{m*}(\Omega_{ij})\, Y_2^m(\Omega_{ij}) = (-1)^m \times 5 \sum_{L=0}^{4} \sqrt{\frac{2L+1}{4\pi}} \times \times \begin{pmatrix} 2 & 2 & L \\ 0 & 0 & 0 \end{pmatrix} \begin{pmatrix} 2 & 2 & L \\ -m & m & 0 \end{pmatrix} Y_L^0(\Omega_{ij}) \quad (9)$$

$\begin{pmatrix} 2 & 2 & L \\ 0 & 0 & 0 \end{pmatrix}$ and $\begin{pmatrix} 2 & 2 & L \\ -m & m & 0 \end{pmatrix}$ are the $3j$ Wigner symbols.

Expression (5) becomes :

$$g_m(0) = 3\pi\hbar^2 \gamma^4 (-1)^m \sum_{L=0}^{4} \sqrt{\frac{2L+1}{4\pi}} \times \times \begin{pmatrix} 2 & 2 & L \\ 0 & 0 & 0 \end{pmatrix} \begin{pmatrix} 2 & 2 & L \\ -m & m & 0 \end{pmatrix} \sum_j \frac{Y_L^0(\Omega_{ij})}{R_{ij}^6} \quad (10)$$

which leads to the expressions :

$$g_0(0) = \frac{M_2}{3} = \frac{3\pi\hbar^2\gamma^4}{\sqrt{4\pi}} \left[ \frac{1}{5} S_0 + \frac{2}{7\sqrt{5}} S_2 + \frac{6}{35} S_4 \right] \quad (11a)$$

$$g_1(0) = \frac{3\pi\hbar^2\gamma^4}{\sqrt{4\pi}} \left[ \frac{1}{5} S_0 + \frac{1}{7\sqrt{5}} S_2 - \frac{4}{35} S_4 \right] \quad (11b)$$

$$g_2(0) = \frac{3\pi\hbar^2\gamma^4}{\sqrt{4\pi}} \left[ \frac{1}{5} S_0 - \frac{2}{7\sqrt{5}} S_2 + \frac{1}{35} S_4 \right] \quad (11c)$$

where the $S_L$ coefficients are defined by the expressions :

$$S_L = \sqrt{\frac{2L+1}{4\pi}} \sum_j \frac{P_L(\Omega_{ij})}{R_{ij}^6} \quad (12a)$$

$P_L(\Omega_{ij})$ is the Legendre polynomial of order $L$. $S_2$ and $S_4$ can be written in terms of the direction cosines $\gamma_x$, $\gamma_y$ and $\gamma_z$ of the magnetic field $H$ relative to the crystal axis. $S_0$ which is proportional to $M_2^0$, the

second moment of the resonant line for a powder, is usually written as

$$S_0 = \frac{1}{\sqrt{4\pi}} \frac{C_6}{a^6}$$

with

$$\frac{C_6}{a^6} = \sum_{i<j} \frac{1}{R_{ij}^6}. \qquad (12b)$$

The calculation yields :

— for the bcc structure [9]

$$S_0 = \frac{1}{\sqrt{4\pi}} \frac{12.25}{a^6} = \frac{5\sqrt{4\pi}}{9\pi\hbar^2\gamma^4} M_2^0 \qquad (13a)$$

$$S_2 = 0 \qquad (13b)$$

$$S_4 = -\frac{1}{\sqrt{4\pi}} \frac{12.8}{a^6}\left(\gamma_x^4 + \gamma_y^4 + \gamma_z^4 - \frac{3}{5}\right) \qquad (13c)$$

— for the hcp structure [9]

$$S_0 = \frac{1}{\sqrt{4\pi}} \frac{14.45}{a^6} = \frac{5\sqrt{4\pi}}{9\pi\hbar^2\gamma^4} M_2^0 \qquad (14a)$$

$$S_2 \simeq 0 \qquad (14b)$$

$$S_4 = \frac{1}{\sqrt{4\pi}} \frac{0.363}{a^6}(35\gamma_z^4 - 30\gamma_z^2 + 3) \qquad (14c)$$

where $\gamma_z$ is the cosine of the angle between H and the trigonal axis. For both structures, $a$ is the nearest neighbour distance between crystalline sites. Using (13) and (14), we find new expressions for (11) :

$$g_0(0) = \frac{M_2^0}{3}\left(1 + \frac{6}{7}\frac{S_4}{S_0}\right) \qquad (15a)$$

$$g_1(0) = \frac{M_2^0}{3}\left(1 - \frac{4}{7}\frac{S_4}{S_0}\right) \qquad (15b)$$

$$g_2(0) = \frac{M_2^0}{3}\left(1 + \frac{1}{7}\frac{S_4}{S_0}\right). \qquad (15c)$$

From (15$a$), we obtain the following useful expressions of $M_2$ :

— bcc structure :

$$M_2 = M_2^0\left\{1 - 0.90\left(\gamma_x^4 + \gamma_y^4 + \gamma_z^4 - \frac{3}{5}\right)\right\} \qquad (16a)$$

— hcp structure :

$$M_2 = M_2^0\{1 + 0.021\,5(35\gamma_z^4 - 30\gamma_z^2 + 3)\}. \qquad (16b)$$

Following Harris, we assume that the spectral densities $J_m(\omega)$ have all the same shape and thus we can write :

$$J_m(\omega) = g_m(0)\,\varphi(\omega) \qquad (17)$$

where $\varphi(\omega)$ contains the informations relative to the dynamics of spins motion and is independent of $m$ under our assumption. We keep the $\varphi(\omega)$ expressions already used for polycrystalline samples [25], [18] :

$$\varphi_{(\omega)}^{ze} = \frac{\sqrt{2\pi}}{\omega_e}\exp\left(\frac{-\omega^2}{2\omega_e^2}\right) \qquad (18a)$$

for hcp structure.

$$\varphi_{(\omega)}^{ze} = \frac{\pi\sqrt{2}}{\omega_e}\exp\left(\frac{-\omega\sqrt{2}}{\omega_e}\right) \qquad (18b)$$

for bcc structure.

Here, $\omega_e/2\pi$ is the exchange frequency defined in both crystalline phases by :

$$\omega_e^2 = \frac{M_4^0}{M_2^0}. \qquad (19)$$

Under the assumption made in this subsection, $\omega_e$ is isotropic and thus $M_2^0$ and $M_4^0$ appearing in (19) are the second and fourth moments for a powder respectively.

3.1.2 Z-VP *regime*. — The study of this relaxation regime can be done either with a classical model [20, 21, 26] where the motion is studied with random functions or with a quantum model where the motion is described by â hamiltonian. The quantum model is performed in reference [19] in a very similar way to the cross relaxation Zeeman-exchange study and leads to a lorentzian spectral density :

$$J_1^v(\omega) = \frac{M_2}{3}\frac{2\tau_v}{1 + \omega^2\tau_v^2}.$$

For a single crystal we assume that the lorentzian shape is conserved and we write :

$$J_m^v(\omega) = g_m(0)\frac{2\tau_v}{1 + \omega^2\tau_v^2} \qquad (20)$$

which is exactly the expression (17) with :

$$\varphi(\omega) = \frac{2\tau_v}{1 + \omega^2\tau_v^2}. \qquad (21)$$

The classical model also makes use of a lorentzian spectral density assumption ; as in (20), we set :

$$J_m^v(\omega) = \lambda g_m(0)\frac{2\tau_v}{1 + \omega^2\tau_v^2}. \qquad (22)$$

The $\lambda$ factor is equal to unity if we use, as in reference [3], the *liquid like* model similar to the model proposed for liquids by Bloembergen, Purcell and Pound [27] and henceforth referred to as the « BPP » model. In that case, $T_1$ minimum (for a powder) is obtained at $\omega\tau_v = 0.615$ and has the value :

$$T_{1\,\min}^{BPP} = \frac{1.05\,\omega}{M_2^0}. \qquad (23)$$

TABLE I

*Maximum values of the $T_1$ and $T_2$ anisotropy factors*

$$K_1 = \frac{\Delta(1/T_1)}{(1/T_1)_{iso}}, K_2 = \frac{\Delta(1/T_2)}{(1/T_2)_{iso}},$$

*according to the relaxation regime and the theory used to describe the motion responsible for the relaxation. We attribute signs to $K_1$ and $K_2$ which account for the relative variation of $T_1$ and $T_2$. In the fourth order theory, $T_1$ and $T_2$ have either in phase variations or opposite phase variations, according to the ratio $\omega/\omega_e$.*

| | Crystalline structure | $K_{1\,max}$ | $K_{2\,max}$ |
|---|---|---|---|
| Z-VP regime | hcp | − (0.062) | + (0.246) |
| Second moment order theory | bcc | + (0.15) | − (0.60) |
| Z-VP regime Random walk + correlation theory, reference [21], table V | bcc | + (0.163) | − (0.47) |
| Z-EP regime | hcp | − (0.164) | + (0.246) |
| Second moment order theory (Harris' results [9]) | bcc | + (0.40) | − (0.60) |
| Z-EP regime | hcp | $-\left(0.189 - 0.049\frac{\omega^2}{2\,\omega_e^2}\right)$ | + (0.283) |
| Fourth moment order theory | bcc | $+\left(0.53 - 0.13\frac{\omega\sqrt{2}}{\omega_e}\right)$ | − (0.80) |

On the other hand, if we use the random walk model [20] for diffusion, henceforth referred to as the *Torrey* model, $\lambda$ is a smooth function of $\omega\tau_v$. A minimum occurs in $T_1$ for $\omega\tau_v = 0.50$ and has the following value for the bcc structure :

$$T_{1\,min}^{T} = \frac{1.144\,\omega}{M_2^0}. \qquad (24)$$

As the expressions (23) and (24) differ by less than 10 %, both models lead to very similar values of $M_2^0$ (see Table II).

In reference [3], eq. ($A_1$.15), the correlation function $\Gamma_{ijij}(t)$ is assumed to be exponential :

$$\Gamma_{ijij}(t) = \Gamma_{ijij}(0)\exp\left(-\frac{t}{\tau_v}\right).$$

This yields eq. (20) directly without further assumption.

Under our assumption (20), all the calculations with $g_m(0)$ made for the Z-EP regime are still valid for the Z-VP regime. We carry out the calculation for both relaxation regimes, each of them being characterized by the $\varphi(\omega)$ expressions (formulae (18*a*) and (18*b*) for the Z-EP regime and formula (21) for the Z-VP regime).

Using formulae (15) and (17), we obtain the general expressions of $T_1$ and $T_2$ valid for both regimes and both crystalline structures :

$$\frac{1}{T_1} = \frac{M_2^0}{3} \times$$

$$\times\left\{\varphi(\omega) + 4\,\varphi(2\,\omega) - \frac{4}{7}\frac{S_4}{S_0}[\varphi(\omega) - \varphi(2\,\omega)]\right\} \qquad (25a)$$

$$\frac{1}{T_2} = \frac{M_2^0}{3}\left\{\frac{3}{2}\varphi(0) + \frac{5}{2}\varphi(\omega) + \varphi(2\,\omega) + \right.$$

$$\left. + \frac{1}{7}\frac{S_4}{S_0}[9\,\varphi(0) - 10\,\varphi(\omega) + \varphi(2\,\omega)]\right\}. \qquad (25b)$$

We define the anisotropy factors $K_1$ and $K_2$ which characterize the amplitude of $T_1$ and $T_2$ variations with $\Theta$ :

$$K_1 = \frac{\Delta(1/T_1)}{(1/T_1)_{iso}}; \qquad K_2 = \frac{\Delta(1/T_2)}{(1/T_2)_{iso}}.$$

$(1/T_1)_{iso}$ and $(1/T_2)_{iso}$ are the isotropic contributions to the relaxation rates,

$\Delta(1/T_1)$ and $\Delta(1/T_2)$ are the differences between the extrema of $(1/T_1)$ or $(1/T_2)$ when the magnetic field orientation $\Theta$ varies through a 180° interval.

They depend on the relative orientations of the rotational axis through the term $S_4$ (see formulae (13*c*) and (14*c*)). The maximal values $K_{1\,max}$ and $K_{2\,max}$ calculated at high frequency ($\omega\tau_v \gg 1$ or $\omega/\omega_e \gg 1$) are reported in table I. We added the results of Wolf [21]

whose theory also predicts and isotropic relaxation at high temperature when $\omega\tau_v \ll 1$. The last part of table I is calculated in the next subsection.

Let us note a consequence of formulae (25) : for both crystalline structures $T_1$ and $T_2$ have opposite variations when the magnetic field orientation changes ; in particular, $T_1$ minimum is expected to correspond to $T_2$ maximum and conversely. Furthermore these features do not change when the Larmor frequency changes, apart from the compensation between $\varphi(0)$, $\varphi(\omega)$ and $\varphi(2\,\omega)$ at low frequency.

3.2 FOURTH ORDER CALCULATION (Z-EP REGIME). — In this subsection, we wish to refine Harris's theory by taking into account the angular variations of the spectral densities $J_m(\omega)$ at non zero frequency $\omega$. We remove the simplifying assumption (17) and allow $\varphi(\omega)$ to depend on the magnetic field orientation. The knowledge of the fourth moment of the resonant line provides some information on the shape of $g_m(t)$ (see eq. (8)). We limit the calculation to the Z-EP regime.

The contribution of the exchange interactions to the fourth moment has been given by Van Vleck [28] when the interaction $J$ is limited to nearest neighbours :

$$M_4 = \gamma^4 \hbar^2 \frac{J^2}{8} \left\{ \sum_{kl} (b_{jl} - b_{kl})^2 + \sum_{jl} (b_{jl} - b_{jk})(b_{jl} - b_{kl}) \right\} \quad (26)$$

with

$$b_{ij} = \frac{3}{2} \frac{\xi(R_{ij})}{R_{ij}^3} (1 - 3\cos^2\theta_{ij})$$

$M_4$ is easily calculated if we take $\xi(R_{ij}) \equiv 1$.

We have performed the calculations for various values of $\theta$ and using $\xi(R_{ij}) = 1$. The results can be written under the same form as $M_2(\theta)$ showing the angular dependence :

— bcc structure :

$$M_4 = (M_2^0 \times 22.8\, J^2) \times \left\{ 1 - 0.304\,5 \left( \gamma_x^4 + \gamma_y^4 + \gamma_z^4 - \frac{3}{5} \right) \right\} \quad (27a)$$

— hcp structure :

$$M_4 = (M_2^0 \times 42\, J^2) \times \{ 1 + 0.014\,95(35\,\gamma_z^4 - 30\,\gamma_z^2 + 3) \}. \quad (27b)$$

The notations are the same as those of eq. (16*a*) and (16*b*). We note that the relative angular variations $\Delta M_4/M_4$ are not negligible at all and that $M_4/M_2$ has an angular dependence which contradicts Harris second order theory. If we try to follow the same method as used in the $M_2$ decomposition, we meet some difficulties : functions $\ddot{g}_m(0)$ contains terms such as

$$\frac{Y_2^m(\Omega_{ij})\, Y_2^{-m}(\Omega_{kl})}{R_{ij}^3 R_{kl}^3} \ddot{\Gamma}_{ij \neq kl}(0)$$

which do not vanish (see Fig. 2*b*). Unlike $g_m(0)$, $\ddot{g}_m(0)$ cannot be written as a sum of spherical harmonics of order 0, 2 and 4. Nevertheless we can still do this decomposition if we only consider *like* terms as $\ddot{\Gamma}_{ijij}(0)$ and neglect the *unlike* terms $\ddot{\Gamma}_{ij \neq kl}(0)$. $\ddot{\Gamma}_{ijij}(0)$ can be calculated using the definition of $\Gamma_{ijkl}(t)$ (eq. (6)) :

$$\ddot{\Gamma}_{ijij}(0) = \frac{N}{\mathrm{Tr}\, I_z^2} \mathrm{Tr}\, [T_{ij}^m, \mathcal{H}_e]\, [\mathcal{H}_e, T_{ij}^m]^\dagger = -3 \sum_k (J_{ik}^2 + J_{jk}^2 + J_{ik} J_{jk}) \quad (28)$$

$J_{ik}$ and $J_{jk}$ are the exchange interaction between spins located on sites $i$ and $k$ or sites $j$ and $k$. In this paper we take $J_{ik} = J$ if sites $i$ and $k$ are nearest neighbours and $J_{ik} = 0$ otherwise as in the $M_4$ calculation (eq. (26)). A calculation very similar to the $g_m(0)$ decomposition leads to the following expressions :

$$\ddot{g}_0^{\text{like}}(0) = \frac{-3\pi\hbar^2\gamma^4}{\sqrt{4\pi}} \left[ \frac{1}{5} U_0 + \frac{2}{7\sqrt{5}} U_2 + \frac{6}{35} U_4 \right] \quad (29a)$$

$$\ddot{g}_1^{\text{like}}(0) = \frac{-3\pi\hbar^2\gamma^4}{\sqrt{4\pi}} \left[ \frac{1}{5} U_0 + \frac{1}{7\sqrt{5}} U_2 - \frac{4}{35} U_4 \right] \quad (29b)$$

$$\ddot{g}_2^{\text{like}}(0) = \frac{-3\pi\hbar^2\gamma^4}{\sqrt{4\pi}} \left[ \frac{1}{5} U_0 - \frac{2}{7\sqrt{5}} U_2 + \frac{1}{35} U_4 \right] \quad (29c)$$

where $U_0$, $U_2$ and $U_4$ are calculated from $\ddot{\Gamma}_{ijij}(0)$ :

$$U_0 = \sqrt{\frac{1}{4\pi}} \sum_j \left\{ \frac{1}{R_{ij}^6} \times \sum_k (J_{ik}^2 + J_{jk}^2 + J_{ik} J_{jk}) \right\} \quad (30a)$$

$$U_2 = \sqrt{\frac{5}{4\pi}} \sum_j \left\{ \frac{3\cos^2\theta_{ij} - 1}{2 R_{ij}^6} \times \sum_k (J_{ik}^2 + J_{jk}^2 + J_{ik} J_{jk}) \right\} \quad (30b)$$

$$U_4 = \sqrt{\frac{9}{4\pi}} \sum_j \left\{ \frac{35\cos^4\theta_{ij} - 30\cos^2\theta_{ij} + 3}{8 R_{ij}^6} \times \sum_k (J_{ik}^2 + J_{jk}^2 + J_{ik} J_{jk}) \right\}. \quad (30c)$$

In the appendix we give some details of the calculation of $U_0$ which contains the contribution $M_4^{0\,\text{like}}$ of the fourth moment in order to compare it to the isotropic part $M_4^0$ of the total fourth moment defined by (26). The unlike contributions to $g_m(t)$ are in

general expected to be small and can then be neglected as for example in the study of the relaxation induced by vacancy motion (see ref. [21] and [26]). Some comments on this assumption will be given later.

Now let us assume that the functions $\ddot{g}_m(0)$ including the unlike terms, can be written in the same form as the functions $\ddot{g}_m^{\text{like}}(0)$, keeping the coefficients of the expansion (29) which are derived from the $3j$ Wigner symbols

$$\ddot{g}_0(0) = -\frac{1}{3} M_4^0 \left\{ 1 + \frac{2\sqrt{5}}{7} \left(\frac{V_2}{V_0}\right) + \right.$$
$$\left. + \frac{6}{7} \left(\frac{V_4}{V_0}\right) \right\} = -\frac{1}{3} M_4 . \quad (31a)$$

This equation defines $V_2/V_0$ and $V_4/V_0$. From (27*a*) and (27*b*) we have :

$\frac{V_2}{V_0} \simeq 0$ for the two crystalline structures

$$\frac{6}{7}\left(\frac{V_4}{V_0}\right) = -0.304\,5\left(\gamma_x^4 + \gamma^y + \gamma_z^4 - \frac{3}{5}\right)$$

for the bcc structure.

$$\frac{6}{7}\left(\frac{V_4}{V_0}\right) = 0.014\,95(35\,\gamma_z^4 - 30\,\gamma_z^2 + 3)$$

for the hcp structure.

We deduce the expression of $\ddot{g}_1(0)$ and $\ddot{g}_2(0)$ :

$$\ddot{g}_1(0) = -\frac{1}{3} M_4^0 \left(1 - \frac{4}{7}\frac{V_4}{V_0}\right) \quad (31b)$$

$$\ddot{g}_2(0) = -\frac{1}{3} M_4^0 \left(1 + \frac{1}{7}\frac{V_4}{V_0}\right). \quad (31c)$$

The expression

$$\omega_m^2 = -\frac{\ddot{g}_m(0)}{g_m(0)} \qquad m = 0, 1, 2 \quad (32)$$

defines three anisotropic frequencies $\omega_m/2\pi$ whose angular variations can be calculated with eq. (15) and (31). As the frequency dependence of $J_m^{ze}(\omega)$ has been measured over four orders of magnitude [25], we believe that this dependence is not appreciably affected by the much smaller angular variations.

Thus we assume that the general form of $\varphi^{ze}(\omega)$ defined by eq. (18*a*) and (18*b*) is still valid but with an anisotropic frequency $\omega_m$ instead of the isotropic one $\omega_e$. This yields :

— for the bcc structure :

$$J_m(\omega) = \pi\sqrt{2}\, g_m(0) \frac{1}{\omega_m} \exp\left(-\frac{\omega\sqrt{2}}{\omega_m}\right) \quad (33)$$

— for the hcp structure :

$$J_m(\omega) = \sqrt{2\pi}\, g_m(0) \frac{1}{\omega_m} \exp\left(-\frac{\omega^2}{2\,\omega_m^2}\right). \quad (34)$$

The explicit expression of $J_m(\omega)$ versus $\theta$ is easy to obtain. The values calculated with the upper and the lower $(V_4/V_0)$ boundaries show that the variations are weak, due to the fact that the $M_2$ and $M_4$ anisotropies partially cancel each other. Thus we are allowed to make a first order expansion in $(V_4/V_0)$ or in $(S_4/S_0)$, which gives clear evidence of the Larmor frequency dependence of the $T_1$ anisotropy. We give the results for the Z-EP regime at high frequency, i.e. when

$$\frac{1}{T_2} \simeq \frac{3}{2} J_0(0) \quad \text{and} \quad \frac{1}{T_1} \simeq J_1(\omega) :$$

— bcc structure :

$$\frac{1}{T_2} \simeq \frac{1}{T_2^0}\left\{1 - 1.2\left(\gamma_x^4 + \gamma_y^4 + \gamma_z^4 - \frac{3}{5}\right)\right. \quad (35)$$

$$\frac{1}{T_1} \simeq \frac{1}{T_1^0}\left\{1 + \left(0.80 - 0.20\,\frac{\omega\sqrt{2}}{\omega_e}\right)\times\right.$$
$$\left.\left. \times \left(\gamma_x^4 + \gamma_y^4 + \gamma_z^4 - \frac{3}{5}\right)\right\}, \quad (36)$$

— hcp structure :

$$\frac{1}{T_2} \simeq \frac{1}{T_2^0}\{1 + 0.024\,7(35\,\gamma_z^4 - 30\,\gamma_z^2 + 3)\} \quad (37)$$

$$\frac{1}{T_1} \simeq \frac{1}{T_1^0}\left\{1 - \left(0.016\,5 - 0.004\,3\,\frac{\omega^2}{2\,\omega_e^2}\right)\times\right.$$
$$\left.\times (35\,\gamma_z^4 - 30\,\gamma_z^2 + 3)\right\}. \quad (38)$$

In these formulae, $T_1^0$ or $T_2^0$ is the isotropic part of $T_1$ or $T_2$ and $\omega_e$ is the isotropic part of the frequencies $\omega_m$ defined above. The new feature predicted by the theory is that the anisotropic contribution to $T_1$ is now frequency dependent and that it changes sign when $\omega$ increases. In table I, we have reported $K_{1\,\max}$ and $K_{2\,\max}$ as calculated from eq. (35) to (38). Comparison with the data is done in the next section.

4. **Experimental results.** — Our data have been obtained with about 60 $^3$He crystals including 25 bcc crystals and 35 hcp crystals. Many hcp crystals had a molar volume close to 19.4 cm$^3$ ; this means that they were grown in the bcc phase and then, during the cooling, they underwent the phase transition bcc-hcp [7], [29]. We might think that this transition had some bearing on the crystal quality ; actually most of these hexagonal crystals (about 90 %) exhibited an anisotropic relaxation which was very similar to the one of samples grown directly in the hcp phase. In order to compare the methods of crystal growth, we also studied four samples (2 in each phase) grown at constant volume by the blocked capillary method and annealed for 2 hours at 30 mK below the melting temperature. Two of them (one cubic and one hexagonal) exhibited an anisotropic relaxation comparable to, although smaller, those of solids grown at constant pressure, whereas no anisotropy was detected

in the last two specimens. It therefore appears that, although good crystals can be obtained by the blocked capillary method, in agreement with reference [8], the result is not as reliable as in the constant pressure method : small crystals with slightly different molar volumes may also be produced in the bulk liquid, giving rise to a poor annealing.

We have tried to measure the thermalization time of vacancies [6]. If we suppose that a vacancy has to move to the crystal surface in order to become annihilated (Schottky defect), we calculate that a waiting time as long as 2 hours is necessary to observe the new equilibrium vacancy population after a change of temperature. We always observed a much shorter thermalization time $T_{th}$; this was determined by measuring $T_1$ rapidly after a sudden change of the temperature. We can place an upper limit of the value of $T_{th}$ of the order of 1 s which was determined by the order of magnitude of $T_1$ and the experimental limits, for instance, the time required to repeat a $T_1$ measurement; actually, it was often unmeasurable with our apparatus. This leads us to think that vacancies are annihilated on dislocation lines rather than the surface [15]. In this connection we note that the *crystal quality*, within the definition given above, is not affected by these defects because the NMR measurements are only governed by the relative orientation of crystals axis and magnetic field. Within the restricted sense of NMR, most of our samples were perfect. This remark is no longer valid at very low temperature and for very pure samples for which it has been suggested that crystal defects may have drastic effects on the relaxation of Zeeman energy towards lattice bath [8]. We present below the detailed analysis of the data of four crystals as typical examples of the experimental features observed with our 60 crystals. We have chosen various domains of molar volumes, temperatures and frequencies in order to give a good account of the large set of data we obtained.

4.1 bcc DATA. — Most of the data have been obtained for crystals having molar volumes close to 20 cm$^3$ and for Larmor frequencies of 3 MHz and 5 MHz. In a large temperature range, the observed relaxation regime is intermediate between the Z-VP regime and the Z-EP regime; it corresponds to the simultaneous modulation of the dipolar hamiltonian by vacancy motion and by exchange. The spectral densities $J_m(\omega)$ are then more complicated than the expressions (18) or (20) standing for a well defined regime. No complete study of the intermediate regime has been made, nevertheless it has been shown that the convolution of the spectral densities $J_m^{v}(\omega)$ and $J_m^{ze}(\omega)$ accounts rather well for the temperature dependence of $T_1$ and $T_2$ [2], [30]. Figure 3 shows the data obtained at Larmor frequency $\omega/2\pi = 5$ MHz, on a sample whose molar volume was $V_m = 19.72$ cm$^3$. In the inset (3*a*) we show the $T_1$ and $T_2$ values measured at $T = 1\,190$ mK, versus

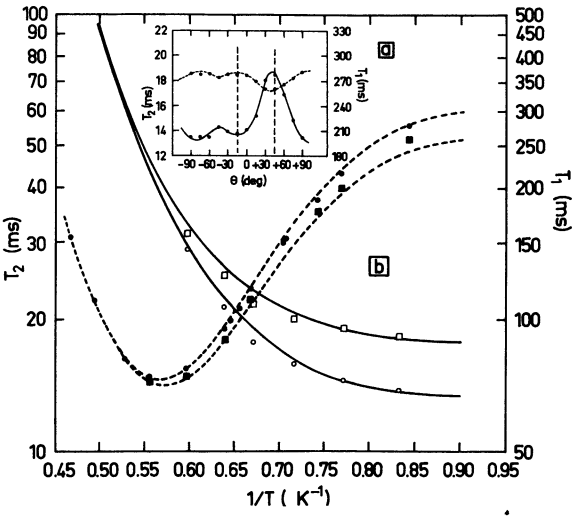


FIG. 3. — Transverse and longitudinal relaxation times of a cubic crystal. $v_m = 19.72$ cm$^3$, $\omega/2\pi = 5$ MHz. (3*a*) shows the angular variations of $T_1$ and $T_2$ at $T \sim 1\,190$ mK. Open circles and the solid curve represent the values of $T_2$. Full circles and the broken curve show the values of $T_1$. Curves are simply an aid to the eye. (3*b*) shows the temperature behaviour of $T_1$ and $T_2$ for the two orientations indicated by the vertical lines in (3*a*). □ for $T_2$ and ■ for $T_1$ correspond to $\theta_2 = +45°$. ○ for $T_2$ and ● for $T_1$ correspond to $\theta_1 = -15°$. The solid curves ($T_2$) and the broken curves ($T_1$) represent the best fits obtained using eq. (25) and a renormalisation factor $\xi_0 = 0.79$ (liquid-like model), as explained in the text. This yields $(S_4/S_0)_{\theta_1} = 0.31$ and $(S_4/S_0)_{\theta_2} = -0.13$.

the rotational angle $\theta$ of the magnetic field $H$. ($\theta = 0$ corresponds to the $H$ direction during the crystal growth.) We note that the opposite variations of $T_1$ versus $T_2$ are in qualitative agreement with formulae (25*a*) and (25*b*). The solid curve and the dashed curve are not mathematical fits but are simply an aid to the eye. [That will also occur in other figures showing $T_1$ or $T_2$ as a function of $\theta$ because, as will be seen in the following discussion, a fit made from expression (25) and the explicit expression of $S_4(\theta)/S_0$ is too unreliable to be useful.]

In figure 3*b* we show the $T_1$ and $T_2$ temperature variations for the same solid and for the two magnetic orientations $\theta_1 = -15°$ and $\theta_2 = +45°$. In this figure, the solid curve and the dashed curve are fits obtained with eq. (25). We are not aware of any published experimental values of $T_1$ near the minimum since the works of Goodkind *et al.* [31] and of Reich [1]. In order to calculate the right $T_1$ minimum we have to take account of the renormalization of the dipolar hamiltonian; this is done by multiplying the second moment $M_2^0$ by a unique factor $\xi_0$. According to the model used to describe the motion of vacancies, two different values of $\xi_0$ are obtained, deduced from either

$$T_{1\,\min}^{BPP} = \frac{1.05\,\omega}{\xi_0\,M_2^0} \quad \text{in the BPP model,}$$

$$T_{1\,\min}^{T} = \frac{1.144\,\omega}{\xi_0\,M_2^0} \quad \text{in the Torrey model.}$$

Table II gives the $\xi_0$ values we obtain using our data and the previously published data [1, 30].

We see that the value of $\xi_0$ are close to one another and that they agree also with a determination [18] obtained by integrating the relaxation rate $T_{ze}^{-1}$ on the Larmor frequency : $0.74 < \xi_0 < 0.89$.

TABLE II

*Renormalization factor $\xi_0$ for the second moment, deduced from the experimental $T_1$ minimum values, according to the model used to describe the atomic motion. In the* BPP *theory* $\xi_0 = 1.05\ \omega/T_{1\min}\ M_2^0$, *while in the theory due to Torrey* $\xi_0 = 1.144\ \omega/T_{1\min}\ M_2^0$. *In reference* [18], *a calculation using the sum rule*

$$\int_0^\infty \frac{d\omega}{T_{ze}} = \pi \xi_0 M_2^0$$

*yields* : $0.74 < \xi_0 < 0.89$ *for a polycrystalline sample.*

| Author | Frequency (MHz) | $T_1$ min (ms) | Theory | $\xi_0$ |
|---|---|---|---|---|
| Goodkind [31] | 30.4 | 420 | BPP [27] (Liquid like) | 0.85 |
| | | | Torrey [20] (Random walk) | 0.92 |
| Reich [1] | 5.224 | 76.3 | BPP | 0.80 |
| | | | Torrey | 0.87 |
| This work | 5 | 72 | BPP | 0.79 ± 0.02 |
| | | | Torrey | 0.86 ± 0.02 |

The $S_4/S_0$ values are deduced from the low temperature values of $T_2$ for each magnetic field orientation ; this yields :

$$\left(\frac{S_4}{S_0}\right)_{\theta_1} = +0.31 \quad \text{and} \quad \left(\frac{S_4}{S_0}\right)_{\theta_2} = -0.13\ .$$

These values are then used to plot the $T_1(T)$ curves.

The atomic jump time $\tau_r$ is supposed to obey an Arrhenius law :

$$\tau_r = \tau_0 \exp\left(\frac{W}{T}\right) \quad \text{with} \quad \tau_r = 2\,\tau_v\ [6]\ .$$

The best fit with the BPP formula (22) yields :

$$\tau_0 = 6.5 \times 10^{-12}\ \text{s}$$

$$W = 15.5\ \text{K}\ .$$

The physical meanings of $\tau_0$ and $W$ are discussed in reference [6]. We believe that $\tau_0$ is accurately measured as it was obtained from a curve with a well defined minimum and was reproducible from run to run. This value does not agree with other published values : $\tau_0 = 10.6 \times 10^{-12}$ s at 30.4 MHz [31] and

$$\tau_0 \simeq 35 \times 10^{-12}\ \text{s}$$

at 80 MHz [6]. Thus, considering that these discrepancies are not likely due to differences in the molar volumes, the experimental $\tau_0$ might increase when the Larmor frequency increases and casts doubts on the validity of the simple lorentzian shape of $J_m^V(\omega)$ at high frequency. The value $\omega_e/2\pi = 2.8$ MHz is used to fit both $T_1$ and $T_2$ data and gives approximatively the right low temperature relaxation times.

We see that the evolution of the $T_2$ anisotropy with temperature is fairly well described by eq. (25*b*) : $K_2$ rises to a maximum at low temperature when $\varphi(0) \gg \varphi(\omega) \gg \varphi(2\,\omega)$ and vanishes at high temperature when the spectral densities $J_0$, $J_1$ and $J_2$ become equal. On the other hand, we note a disagreement in the temperature range around 1 600 mK :

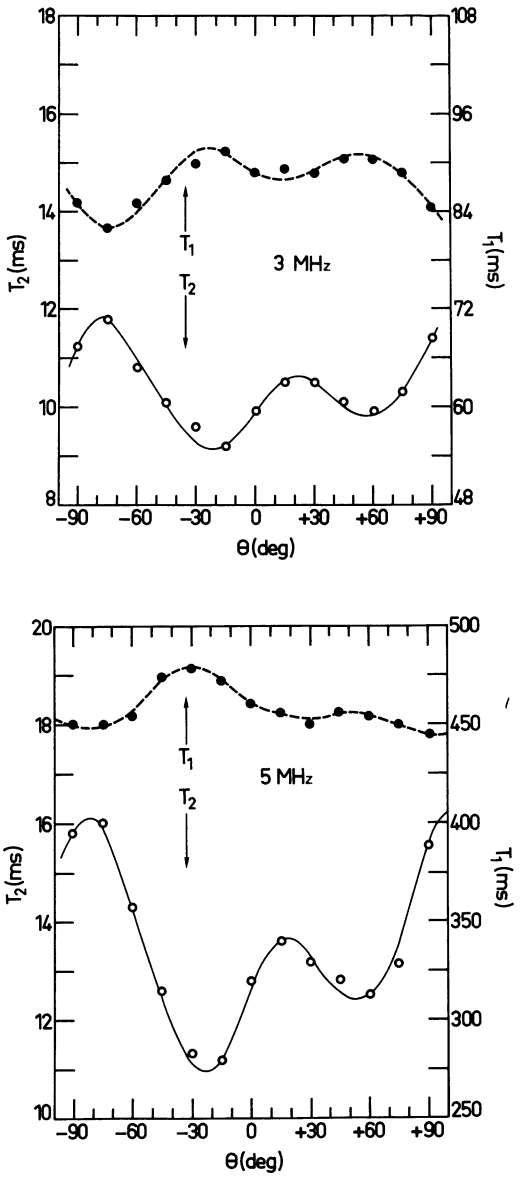


FIG. 4. — Variation of $T_1$ and $T_2$ with the direction $\theta$ of the magnetic field measured at frequencies 3 MHz and 5 MHz, for a cubic crystal $V_m = 19.55$ cm$^3$, $T = 1\,180$ mK. Open circles are $T_2$ values and full circles are $T_1$ values. Solid curves and broken curve are added to aid the eye.

when the functions $J_1$ and $J_2$ become much smaller than $J_0$, the $\frac{10}{3}$ *effect* [4], although reduced by the exchange effect, yields an inflection in the theoretical curves which is observed neither in the data nor in the results available in the literature [2, 3]. The temperature variations of $T_1$ calculated with the convolution of the spectral densities $J_m^{v}(\omega) \circledast J_m^{ze}(\omega)$ agree fairly well with the data, in contrast to the anisotropy factor $K_1$ calculated from eq. (25*a*) which is equal to 0.16 at 1 190 mK while the experimental value is

$$K_{1\,\mathrm{exp}} = 0.08 .$$

This kind of disagreement was observed in all bcc samples studied at 5 MHz.

Figure 4 shows the anisotropic $T_1$ and $T_2$ in a cubic crystal of molar volume $V_m = 19.55$ cm$^3$ measured at two Larmor frequency $\omega/2\pi = 3$ MHz and 5 MHz. We observe again that the longitudinal and transverse relaxation times have opposite variations with $\theta$, but the new interesting feature is that the curve $T_1 = f(\theta)$ has a frequency dependent shape. Furthermore, the anisotropic factor $K_1$ varies from 0.08 at 5 MHz to 0.11 at 3 MHz, in disagreement with eq. (25*a*) which predicts that $K_1$ (3 MHz) < $K_1$ (5 MHz) because the ratio $J_2(2\omega)/J_1(\omega)$ increases when the Larmor frequency decreases. Now, let us apply the results of the fourth order theory to the crystal of figure 4 :

— at 5 MHz

$$\frac{\omega\sqrt{2}}{\omega_e} \simeq 3.1 .$$

Eq. (36) yields :

$$\frac{1}{T_1} \simeq \frac{1}{T_1^0}\left\{1 + 0.18\left(\gamma_x^4 + \gamma_y^4 + \gamma_z^4 - \frac{3}{5}\right)\right\}$$

while $1/T_2$ is still given by (35) ;

— at 3 MHz

$$\frac{1}{T_1} \simeq \frac{1}{T_1^0}\left\{1 + 0.43\left(\gamma_x^4 + \gamma_y^4 + \gamma_z^4 - \frac{3}{5}\right)\right\}$$

while the expected $(1/T_2)$ anisotropy is reduced by the compensation between $J_0(0)$ and $J_1(\omega)$.

Eq. (36) therefore provides a good account of the $K_1$ behaviour when $\omega$ decreases : $K_1$ increases but remains smaller than $K_2$. The same feature applies to the crystal of figure 3 and may explain the discrepancy of the $T_1$ anisotropy fit at low temperature.

4.2 hcp DATA. — Figure 5 shows the anisotropic relaxation times of a hcp monocrystal ($V_m = 19.46$ cm$^3$) measured at four Larmor frequencies :

$$\frac{\omega}{2\pi} = 5 \text{ MHz}, 3 \text{ MHz}, 2.125 \text{ MHz and } 1.5 \text{ MHz} .$$

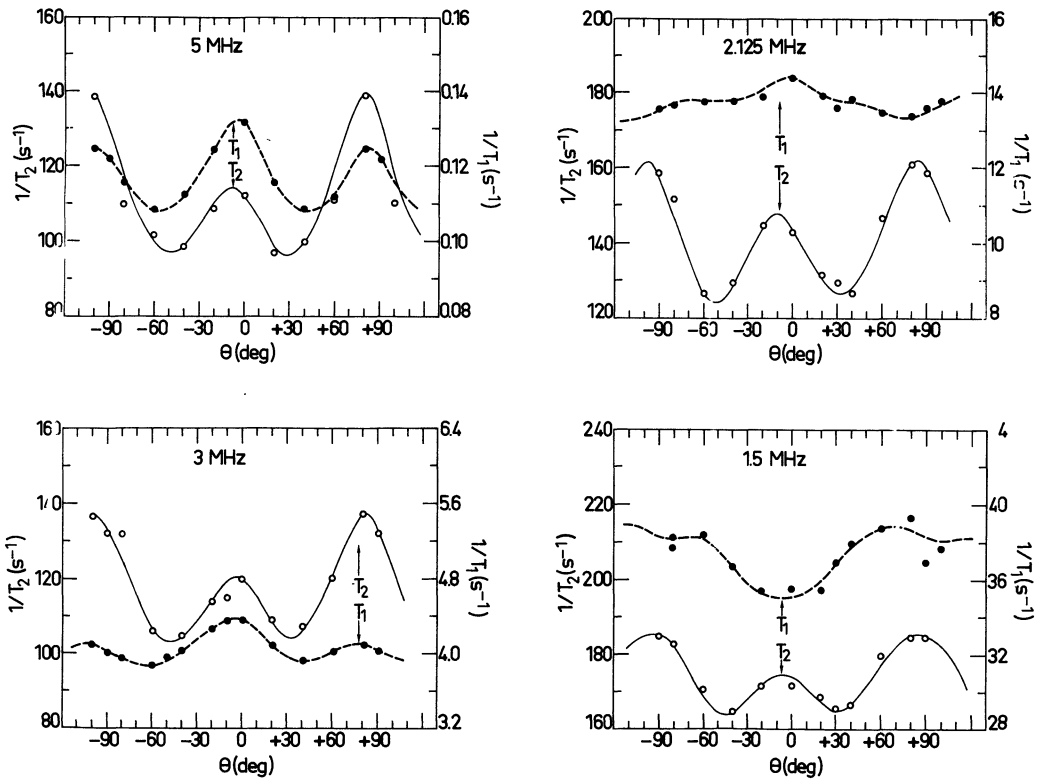


FIG. 5. — Variations of $T_1$ and $T_2$ with the direction $\theta$ of the magnetic field measured for the same hexagonal crystal $V_m = 19.46$ cm$^3$, at the four frequencies 5 MHz, 3 MHz, 2.125 MHz and 1.5 MHz and at $T = 1\,180$ mK. For each frequency data, open circles represent values of $1/T_2$ and full circles indicate values of $1/T_1$. The solid curves and the broken curves are simply an aid for the eye.

The $T_2$ features are in qualitative agreement with formulae (37) or (25*b*) which predict no frequency dependence for $T_2$ apart from the decrease of $K_2$ at low frequency due to the compensation between the spectral densities. Let us make a short comment on the shape of the $T_2(\theta)$ curve. Eq. (14*c*) shows that the orientation of the crystal trigonal axis can be roughly estimated by inspection of the curve $T_2(\theta)$. If we call $\phi$ the angle between the trigonal axis and the rotational axis of the magnetic field, the direction cosine $\gamma_z$ is : $\gamma_z = \cos(\theta - \theta_0) \sin\phi$, where $\theta_0$ is an arbitrary origine for $\theta$. When $\theta$ varies from $-\pi/2$ to $\pi/2$, $S_4(\theta)$ exhibits two maxima and two minima if $\sin\phi > 0.7$ and only one maximum and one minimum otherwise. Almost all our samples presented $T_2(\theta)$ curves similar to that of figure 5 which corresponds to $\sin\phi \neq 1$. It seems clear that hexagonal crystals have a pronounced tendency to grow with their trigonal axes perpendicular to the temperature gradient (which is parallel to the magnetic field rotation axis in our apparatus). This feature agrees with more precise orientation determinations made by Greywall with the use of X-rays [13].

The remarkable feature of figure 5 is the drastic change in the curves $T_1(\theta)$ when the Larmor frequency varies : $T_1$ and $T_2$ have in phase variations at high frequency, this is no more true at 2.125 MHz and the $T_1(\theta)$ shape becomes more complicated at 1.5 MHz. This $T_1$ behaviour was not expected by the second order theory but the fourth order theory allows $K_1$ to change sign when the frequency varies (see formula (38)). As we did for the bcc sample, we apply this last theory to the hexagonal sample of figure 5 :

— at 5 MHz

$$\frac{\omega^2}{2\,\omega_e^2} \simeq \ln\left(\frac{2}{3}\frac{T_1}{T_2}\right) \simeq 6.5$$

$$\frac{1}{T_1} \simeq \frac{1}{T_1^0}\{1 + 0.011\,5(35\,\gamma_z^4 - 30\,\gamma_z^2 + 3)\}$$

$1/T_2$ has the expression (37),

— at 3 MHz

$$\frac{1}{T_1} \simeq \frac{1}{T_1^0}\{1 - 0.006\,5(35\,\gamma_z^4 - 30\,\gamma_z^2 + 3)\}$$

while $1/T_2$ is almost not affected.

The agreement with data is not quantitatively correct as the experimental $T_1$ and $T_2$ do not have opposite phase variations at 3 MHz; nevertheless eq. (38) gives a good account for the decrease of $T_1$ anisotropy when $\omega$ becomes smaller than 5 MHz.

We should mention some measurements made in the temperature range covering the transition between the Z-EP regime and the Z-VP regime. Figure 6 shows the variations of the anisotropy of $T_1$ for a hcp crystal of molar volume $V_m = 19.15$ cm$^3$ measured at 3 MHz when the temperature varies between 1 190 mK and 2 415 mK. While $K_1$ varies from 0.19 at 1 190 mK to less than 0.04 at 2 415 mK, we see that a single temperature independent curve A($\theta$) accounts satisfactorily for the $1/T_1$ anisotropy throughout the entire temperature range. We can thus write :

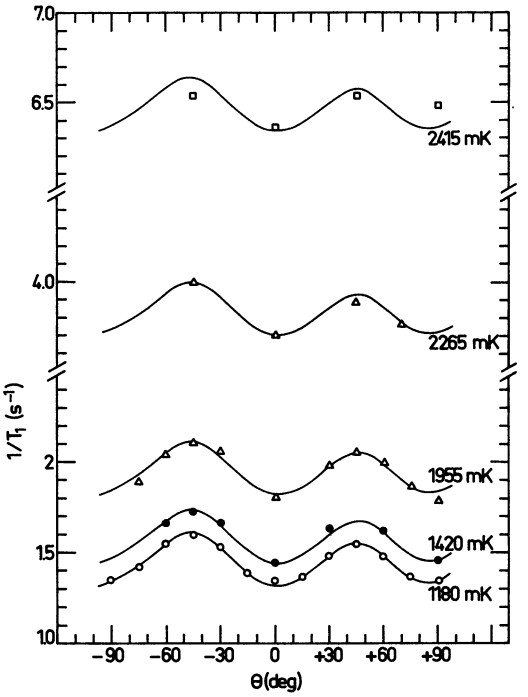


FIG. 6. — Variations of $1/T_1$ with magnetic field orientation for a hexagonal crystal $V_m = 19.15$ cm$^3$, measured at Larmor frequency 3 MHz, in a temperature range covering the transition from the exchange induced relaxation regime (low temperature) to the vacancy induced relaxation regime (high temperature). The solid curve $B(\theta)$ which passes through the data at 1180 mK is simply translated for the other temperature data and illustrates the equation : $1/T_1 = A(T) + B(\theta)$.

$$\frac{1}{T_1} = A(\theta) + B(T)$$

where $B(T)$ stands for an isotropic but temperature dependent variation of $1/T_1$. We might interpret $A(\theta)$ as the exchange contribution to the relaxation and $B(T)$ as the contribution due to vacancies; but, when considering all the approximations made in the fourth order theory, we believe that the measurements reported in figure 6 cannot lead to a clear understanding of the transition between the two relaxation regimes.

Actually, many experimental features are not explained by the theory. In the Z-EP regime, the expected $K_{2max}$ is equal to 0.283 while the measured $K_2$ at 5 MHz is always larger than 0.30 (in Fig. 5, it is equal to 0.35). Furthermore, the theory does not explain why the shape of the curve $T_1(\theta)$ varies with $\omega$. For these reasons, we have not tried to obtain a precise fit of the theory to experiment, using for

instance eq. (37) and (38) to calculate $T_1(\theta)$ and $T_2(\theta)$. Since the fourth order theory gives only a qualitative account of the change of the anisotropy of $T_1$ with frequency, such a fit would not have been very convincing and consequently it has not been reported in this paper. We believe that the failure of the theory to explain the change of the shape of the curve $T_1(\theta)$ arises when we assume that $\ddot{g}_m(0)$ can be written in the same form as $\ddot{g}_m^{\text{like}}(0)$ (eq. (29) and (31)). This means that we assume that $\ddot{g}_m(0)$ can be expanded with Legendre polynomials of order 0.2 and 4, when the exact form of $\ddot{g}_m(0)$ is certainly more complex. Such an assumption should be removed in a refined theory.

5. **Conclusion.** — The experimental data presented in this paper show that it is possible to grow single $He^3$ crystals using relatively simple techniques and to study their anisotropic nuclear relaxation. Actually this is not a new experiment as single $He^3$ crystals have been grown for a long time in other kinds of measurements and nuclear relaxation has been extensively measured since the beginning of the study of solid $^3He$; the essential new feature is NMR measurements related to single crystals. In some ways our data suggests that studies of the anisotropies are not very useful in NMR experiments : all the previous features calculated or observed with a powder still stand for a single crystal and it is not important to know whether the sample is a single crystal or not, at least in the two relaxation regimes dealt with in this paper. On the other hand, the positive outcome of this work is the determination of the order of magnitude of the relaxation times anisotropies. Care has been taken not to attribute some discrepancy in the analysis of the results with uncertainties in the crystal quality; we refer in particular to the determination of $\tau_0$ which varies by a factor 6 according to whether it is measured at 5 MHz or at 80 MHz (see section 4). Our results show that this feature cannot be accounted for by a powder versus single crystal effect.

From the point of view of NMR, we have pointed out the frequency dependence of the anisotropies of the spectral densities $J_1(\omega)$ and $J_2(2\omega)$ in both crystalline structures. Nevertheless, our model which gives only a phenomenological definition of the anisotropic frequencies $\omega_m$ is too approximative to be correct throughout a large frequency range : in particular, eq. (33) and (34) are probably invalid for large values of $\omega/\omega_e$. The application of the theory to the Z-VP regime is also open to criticism and, apart from the high temperature isotropy of the relaxation times, its other predictions have not been verified satisfactorily. Some further experiments might also be useful in order to test the validity of the approximation usually made in the study of the relaxation induced by translational diffusion, which is to neglect the unlike terms of the correlation function $\Gamma_{ijkl}(t)$ (see ref. [21], eq. (2.1) and ref. [26], eq. (8)). Under examination of the contribution of the exchange interaction to the fourth moment, we see that $M_4^{0\text{like}}$, as calculated in the appendix, is 24 % and 37 % larger than $M_4^{0\text{total}}$, in the hcp phase and in the bcc phase respectively. These differences are significant and the unlike terms cannot be ignored in the study of the Z-EP regime. In the Z-VP regime, the complete calculation should be a difficult task and the modifications to the present theory should probably be small because the anisotropy associated with the motion of vacancies is small in the two phases. For the sake of completeness, the $M_2$ and $M_4$ calculations could be repeated with a nontrivial renormalization function $\xi(R_{ij})$; furthermore the anisotropy of the fourth moment should be calculated including the contribution of the next nearest neighbour exchange [18]. Our feeling is that these refinements cannot be introduced within our phenomenological model of section 3 but require the framework of a new treatment of the relaxation mechanism starting from the general expression of $g_m(t)$ which should not use the phenomenological expressions of $\varphi(\omega)$ such as (18*a*) and (18*b*). These expressions are based on experimental values and their validity has been recently contested by measurements [32] in the bcc phase at high frequency. Study of the anisotropy of the relaxation rates might help to elucidate the physical origin of the difference between the gaussian shape of the hcp spectral density and the exponential shape of the bcc one.

**Acknowledgments.** — I wish to thank G. Delmas for his aid with the construction of the constant pressure cell and M. Bernier who designed the very reliable pulsed NMR spectrometer. I especially acknowledge A. Landesman for his constant aid and interest in each step of this work and also M. Goldman, D. Marty, N. Sullivan and F. I. B. Williams for enlightening discussions and critical reading of the manuscript.

**Appendix : Contribution of *like* terms to the fourth moment when exchange relaxation is dominant.** — The fourth moment is expressed in terms of the four spin correlation function $\Gamma_{ijkl}(t)$ :

$$M_4 = -\frac{12\,\pi\hbar^2\,\gamma^4}{5\,N}\sum_{i<j}\sum_{k<l}\frac{Y_2^0(\Omega_{ij})\;Y_2^0(\Omega_{kl})}{R_{ij}^3\,R_{kl}^3}\,\ddot{\Gamma}_{ijkl}(0)\,.$$

We define as $M_4^{\text{like}}$, the quantity obtained when the unlike terms $\ddot{\Gamma}_{ij\neq kl}(0)$ are neglected

$$M_4^{\text{like}} = -\frac{12\,\pi\hbar^2\,\gamma^4}{5\,N}\sum_{i<j}\frac{[Y_2^0(\Omega_{ij})]^2}{R_{ij}^6}\,\ddot{\Gamma}_{ijij}(0)\,. \quad \text{(A.1)}$$

Following the definition (6) of $\Gamma(t)$, $\ddot{\Gamma}_{ij,ij}$ is expressed in terms of the exchange hamiltonian $\mathcal{H}_e$ :

$$\ddot{\Gamma}_{ijij}(0) = \frac{N}{\text{Tr}\,I_z^2}\,\text{Tr}\,[T_{ij}^m,\,\mathcal{H}_e]\,[\mathcal{H}_e,\,T_{ij}^m]^+ \quad \text{(A.2)}$$

which is $m$ independent (see section 3). We calculate $\ddot{\Gamma}_{ijij}(0)$ using $m = 2$

$$[T_{ij}^2, \mathcal{H}_e] = \left(-\sqrt{\frac{3}{2}}\right)(-2J_{ij})[I_i^+ I_j^+, \mathbf{I}_i \mathbf{I}_j] + \\ + \sum_k \left(-\sqrt{\frac{3}{2}}\right)(-2)[I_i^+ I_j^+, \mathbf{I}_k.(\mathbf{I}_i J_{ik} + \mathbf{I}_j J_{jk})] .$$

The first term gives zero, we get :

$$[T_{ij}^2, \mathcal{H}_e] = \sqrt{6} \sum_k \{ J_{ik} I_j^+ (I_i^z I_k^+ - I_i^+ I_k^z) + \\ + J_{jk} I_i^+ (I_j^z I_k^+ - I_j^+ I_k^z) \} .$$

After straightforward calculations, eq. (A.2) becomes :

$$\ddot{\Gamma}_{ijij}(0) = -3 \sum_k (J_{ik}^2 + J_{jk}^2 + J_{ik} J_{jk})$$

and from (A.1) we get :

$$M_4^{\text{like}} = \frac{36\pi}{10} \hbar^2 \gamma^4 \sum_j \frac{[Y_2^0(\Omega_{ij})]^2}{R_{ij}^6} \times \\ \times \sum_k (J_{ik}^2 + J_{jk}^2 + J_{ik} J_{jk}) .$$

We calculate the isotropic part $M_4^{0\,\text{like}}$ of $M_4^{\text{like}}$, which is proportional to $U_0$ defined in (30*a*) :

$$M_4^{0\,\text{like}} = \frac{9}{10} \hbar^2 \gamma^4 \sum_j \frac{1}{R_{ij}^6} \sum_k (J_{ik}^2 + J_{jk}^2 + J_{ik} J_{jk}) .$$

We write

$$M_4^{0\,\text{like}} = \frac{9}{10} \hbar^2 \gamma^4 (A + B)$$

$$A = \sum_j \frac{1}{R_{ij}^6} \sum_k (J_{ik}^2 + J_{jk}^2)$$

$$B = \sum_j \frac{1}{R_{ij}^6} \sum_k (J_{ik} J_{jk}) .$$

We limit the exchange interactions to the $n$ nearest neighbours

($n = 12$ for hcp and $n = 8$ for bcc) .

The $k$ summation in $A$ gives $2nJ^2$ excepted when $k$ is identical to $i$ or $j$

$$A = \frac{J^2}{a^6} \left\{ \left[ 2n \times \sum_j \left( \frac{a}{R_{ij}} \right)^6 \right] - 2n \right\}$$

$$A = 2n \frac{J^2}{a_6} (C_6 - 1)$$

where $C_6$ [18] is the numerical coefficient defined by (12*b*)

$$C_6^{\text{bcc}} = 12.25$$

$$C_6^{\text{hcp}} = 14.45 .$$

For the $B$ evaluation, we need to consider the isoceles triangles $kij$ in which $k$ is nearest neighbour of $i$ and $j$ and thus the distance $R_{ij}$ obeys to :

$$a < R_{ij} \leqslant 2a .$$

We give for each crystalline structure the values of the successive nearest distances $R_{ij}$, the number $m$ of the corresponding sites $j$ neighbours of site $i$, the number $p$ of isoceles triangles $kij$ made with a pair $ij$, the total number of triangles involved in the summation for each distance $R_{ij}$ being the product $mp$.

bcc *structure*

| $R_{ij}$ | $m$ | $p$ |
|---|---|---|
| $a\sqrt{\frac{4}{3}}$ | 6 | 4 |
| $a\sqrt{\frac{8}{3}}$ | 12 | 2 |
| $2a$ | 8 | 1 |

we obtain : $B^{\text{bcc}} = 11.515 \dfrac{J^2}{a^6}$ .

hcp *structure*

| $R_{ij}$ | $m$ | $p$ |
|---|---|---|
| $a$ | 12 | 4 |
| $a\sqrt{2}$ | 6 | 4 |
| $a\sqrt{\frac{8}{3}}$ | 2 | 3 |
| $a\sqrt{3}$ | 18 | 2 |
| $a\sqrt{\frac{11}{3}}$ | 12 | 1 |
| $2a$ | 6 | 1 |

we obtain : $B^{\text{hcp}} = 52.987 \dfrac{J^2}{a^6}$ .

Combining $A$ and $B$ results, we get the final expression of $M_4^{0\,\text{like}}$ :

— bcc structure

$$M_4^{0\,\text{like}} = \frac{9}{10} \hbar^2 \gamma^4 \frac{J^2}{a^6} \{ 16 \times (12.25 - 1) + 11.515 \}$$

or

$$M_4^{0\,\text{like}} = 31.27\, M_2^0\, J^2$$

to be compared to

$$M_4^{0\,\text{total}} = 22.8\, M_2^0\, J^2 \quad \text{(see formula (26))}$$

— hcp structure

$$M_4^{0\,\text{like}} = \frac{9}{10} \hbar^2 \gamma^4 \frac{J^2}{a^6} \{ 24 \times (14.45 - 1) + 52.987 \}$$

or :

$$M_4^{0\,\text{like}} = 52.01\, M_2^0\, J^2$$

to be compared to

$$M_4^{0\,\text{total}} = 42\, M_2^0\, J^2 \quad \text{(see formula (27))}.$$

## References


[1] GARWIN, R. L. and REICH, H. A., *Phys. Rev.* **115** (1959) 1478. REICH, H. A., *Phys. Rev.* **129** (1963) 630.

[2] GARWIN, R. L. and LANDESMAN, A., *Phys. Rev.* **133A** (1964) 1503.

[3] GUYER, R. A., RICHARDSON, R. C. and ZANE, L. I., *Rev. Mod. Phys.* **43** (1971) 532 and references therein.

[4] VOS, J. E., BLAISSE, B. S., BOON, D. A. E., VAN SCHERPENZEEL, W. J. and KINGMA, R., *Physica* **37** (1967) 51.
VOS, J. E. and KINGMA, R., *Cryogenics* **7** (1967) 50.
VOS, J. E., VEENENGA KINGMA, R., VAN DER GAAG, F. J. and BLAISSE, B. S., *Phys. Lett.* **24A** (1967) 738.

[5] RICHARDS, M. G., HATTON, J. and GIFFARD, R. P., *Phys. Rev.* **139A** (1965) 91.
RICHARDSON, R. C., HUNT, E. and MEYER, H., *Phys. Rev.* **138A** (1965) 1326.
RICHARDSON, R. C., LANDESMAN, A., HUNT, E. and MEYER, H., *Phys. Rev.* **146** (1966) 244.

[6] SULLIVAN, N., DEVILLE, G. and LANDESMAN, A., *Phys. Rev.* **11B** (1975) 1858.

[7] GRILLY, E. R. and MILLS, R. L., *Ann. Phys.* (NY) **8** (1959) 1.

[8] GIFFARD, R. P., TRUSCOTT, W. S. and HATTON, J., *J. Low Temp. Phys.* **4** (1971) 153.

[9] HARRIS, A. B., *Solid State Commun.* **9** (1971) 2255.

[10] TRUSCOTT, W. S., Thesis Oxford (1972) (unpublished).

[11] MEZHOV-DEGLIN, L. P., *Zh. Eksp. Teor. Fiz.* **49** (1965) 66; (*Sov. Phys. JETP* **22** (1966) 47).

[12] CREPEAU, R. H., HEYBEY, O., LEE, D. M. and STRAUSS, S. A., *Phys. Rev.* **3A** (1971) 1162.

[13] GREYWALL, D. S., *Phys. Rev.* **3A** (1971) 2106.

[14] See also the review of properties of solid helium in : TRICKEY, S. B., KIRK, W. P. and ADAMS, E. D., *Rev. Mod. Phys.* **44** (1972) 668.

[15] MARTY, D. and WILLIAMS, F. I. B., *J. Physique* **34** (1973) 989.

[16] HAHN, E., *Phys. Rev.* **80** (1950) 580.

[17] ABRAGAM, A., *The principles of nuclear magnetism* (Oxford U.P. Oxford, England) 1961, Chap. III.

[18] LANDESMAN, A., *Ann. Phys.* (Paris) **8** (1974) 53.

[19] LANDESMAN, A., *Ann. Phys.* (Paris) **9** (1975) 69.

[20] TORREY, H. C., *Phys. Rev.* **92** (1953) 962.
RESING, H. A. and TORREY, H. C., *Phys. Rev.* **131** (1963) 1102.

[21] WOLF, D., *Phys. Rev.* **10B** (1974) 2710.

[22] WOLF, D., *J. Magn. Res.* **17** (1975) 1.

[23] Ref. [17] Chap. IV.

[24] MESSIAH, A., *Mécanique quantique* Tome II (Dunod) Paris, 1960.

[25] THOMLINSON, W. C., KELLY, J. F. and RICHARDSON, R. C., *Phys. Lett.* **38A** (1972) 531.

[26] EISENSTADT, M. and REDFIELD, A. G., *Phys. Rev.* **132** (1963) 635.

[27] BLOEMBERGEN, N., PURCELL, E. M. and POUND, R. V., *Phys. Rev.* **73** (1948) 679.

[28] VAN VLECK, J. H., *Phys. Rev.* **74** (1948) 1168.

[29] STRATY, G. C. and ADAMS, E. D., *Phys. Rev.* **169** (1968) 232.

[30] HARTMANN, S. R., *Phys. Rev.* **133A** (1964) 17.

[31] GOODKIND, J. M. and FAIRBANK, W. M., *Phys. Rev. Lett.* **4** (1960) 458.

[32] SULLIVAN, N. and CHAPELLIER, M., *J. Phys. C* **7** (1974) L195.